PCCP

Accepted Manuscript

This article can be cited before page numbers have been issued, to do this please use: Z. Gao, W. Yang, X. Ding, G. Lv and W. Yan, *Phys. Chem. Chem. Phys.*, 2018, DOI: 10.1039/C7CP08301G.

View Article Online
DOI: 10.1039/C7CP08301G

Physical Chemistry Chemical Physics

ARTICLE

Support effects on adsorption and catalytic activation of O_2 in single atom iron catalysts with graphene-based substrates

Received 00th January 20xx,
Accepted 00th January 20xx

DOI: 10.1039/x0xx00000x

www.rsc.org/

Zheng-yang Gao[a], Wei-jie Yang[a*], Xun-lei Ding[b*], Gang Lv[c] and Wei-ping Yan[a]

The adsorption and catalytic activation of O_2 on single atom iron catalysts with graphene-based substrates were investigated systematically by density functional theroy calculation. It is found that support effects of graphene-based substrates have significant influence on the stability of single atom catalysts, adsorption configuration, electron transfer mechanism, adsorption energy and energy barrier. The difference of stable adsorption configuration of O_2 on single atom iron catalysts with different graphene-based substrates can be well understood by symmetrical matching principle based on frontier molecular orbital analysis. There are two different mechanisms of electron transfer，in which Fe atom acts as electron donor in single vacancy graphene-based substrates while Fe atom mainly acts as the bridge of electron transfer in double vacancy graphene-based substrates. Fermi softness and work function are good descriptors of adsorption energy and they can well reveal the relationship between electronic structure and adsorption energy. Single atom iron catalyst with single vacancy graphene modified by three nitrogen atom is a promising non-noble metal single atom catalyst in adsorption and catalytic oxidation of O_2. Furthermore, the findings can lay a foundation for the further study of graphene-based support effects and provide a guideline for development and design of new non-noble-metal single atom catalysts.

1. Introduction

Single atom catalysts (SACs) have attracted increasing attention in the field of heterogeneous catalysis owing to their high catalytic activity and high selectivity. As a type of novel heterogeneous catalyst, SACs promise to become a bridge between homogeneous and heterogeneous catalysis and show super catalytic activity in many industrial catalytic reactions, such as CO oxidation[1-3] , water-gas shift [4, 5], carbon dioxide reduction [6], hydrogen evolution reaction [7] and oxygen evolution reaction [8, 9]. As the size of catalyst becomes smaller and smaller, the stability of catalyst becomes more and more difficult to guarantee, indicating that substrates should firmly anchor the metal atom and avoid the occurrence of metal atom agglomeration[10]. The interaction between pristine graphene and metal atom is relatively weak[11], while the vacancy of defective graphene[12] and graphyne[13] can firmly anchor metal atom. Therefore, graphene with vacancy defects can be an excellent support for SACs for its anchor effect, large specific surface area and unique physicochemical properties [14,15].

SACs which are synthesized by embedding non-noble-metal atoms in graphene-based substrates (M/GS) can further reduce the cost of catalysts, and a large number of theoretical and experimental studies on TM/GS have been performed. [16-20]. Previous researches suggested that Fe/GS has high adsorption activity for toxic gases, such as CO[21], NO[22], HCN[23], SO_2[24] and NH_3[25]. Furthermore, the catalytic performance of Fe/GS in oxygen reduction reaction can come up to the noble metals of Pd and Pt[8, 26].Therefore, Fe as a kind of non-noble-metal can be the catalyst atom of SACs, and Fe/GS is a promising catalyst. However, there are also many worthy of further research and exploration, such as support effects [27], synthesis and preparation [28, 29].

The adsorption and activation of O_2 on catalysts surface can be considered as the essential step of a variety of reaction processes [30], such as CO oxidation [31, 32] and oxygen reduction reaction [33]. Zhang et al. investigated the adsorption of O_2 on Au/GS under an external electric field and found that the mechanism of electron transfer between O_2 and Au/GS can be modulated by external electric field. Liu et al. studied the catalytic oxidation of O_2 on Pt/GS and Pt_4/GS and concluded that the positive polarized charges of Pt can significantly decrease dissociation barrier of O_2 [34]. However, up to date, there is limited investigation insight into the detailed adsorption and catalytic activation of O_2 on Fe/GS. Therefore, the interaction between O_2 and Fe/GS deserves comprehensive investigations to realize the design and application of low price and high efficiency catalyst.

SACs belong to supported catalyst, and the supports of catalysts have a significant influence on catalysis activity [27, 35]. The researches of support effects on single atom catalysts are

[a] School of Energy and Power Engineering, North China Electric Power University, Baoding 071003, China.
[b] School of Mathematics and Physics, North China Electric Power University, Beijing 102206, China.
[c] School of Mathematics and Physics, North China Electric Power University, Baoding 071003, China.
E-mail: yangwj@ncepu.edu.cn or dingxl@ncepu.edu.cn. Fax: +86 0312 7522681; Tel: +86 0312 7522681

View Article Online
DOI: 10.1039/C7CP08301G

still relative insufficient, and most of investigations are focused on the supports of metal oxides. Wang et al. investigated the effect of support phase transition on Rh_1/VO_2 catalyzing ammonia–borane hydrolysis, and results suggested that band structure of support will affect the catalytic activity of Rh_1/VO_2 by influencing the highest electron occupancy state of Rh atom[35]. Tang et al. studied the adsorption characteristics of CO on Au_1/MO_2 and Au_1/MO_{2-x} (M=Ti, Zr, Ce, Hf, Th), and they concluded that quantum primogenic effect plays a critical role in the adsorption modes of CO on various MO_2 supports [27]. Comparing the oxidation of CO on single Pt atom catalyst with different graphene-based substrates[36-38], we can conclude that support effects of graphene-based substrates have obvious influence on catalytic activity of SACs. Furthermore, the same catalytic reactions on metal nanoparticles supported with different graphene-based substrates show remarkably different energy barriers which also confirm the importance of support effects[39, 40]. However, there is limited study insight into support effects of graphene-based substrates on the adsorption and activation of O_2 in TM/GS, although the support effect is known to be a key factor in determining the structural and chemical properties of TM/GN catalysts. Therefore, it is imperative to systematically study the adsorption and reaction mechanism of O_2 molecule on Fe/GS to reveal the nature of support effect of graphene-based substrates.

Taking into account the catalyst preparation in practical, vacancy defects and nitrogen doping are common and accessible modification method, ten kinds of graphene-based substrates were constructed through vacancy defects and nitrogen doping to systematically study the support effects of graphene-based substrates on adsorption and catalytic activation of O_2 molecule. Firstly, end-on and side-on adsorption configurations of O_2 molecule on Fe/GS were optimized. The electron transfer mechanism under side-on and end-on adsorption model was analyzed, and the relationship between adsorption and bond length of O_2 was discussed. Secondly, the frontier molecular orbital method was applied to reveal the most stable adsorption of O_2 on Fe/GS. Thirdly, Fermi softness and work function of Fe/GS were calculated to deepen the understanding of the relationship between adsorption energy and electron structure of Fe/GS. Finally, the energy barrier of O_2 dissociation was obtained through transition state calculation to further examine the catalytic activity of Fe/GS. The present investigation can provide new insights for understanding support effects of graphene-based substrates and designing new non-noble-metal single atom catalysts.

2. Calculation method

All calculations were performed using Vienna *ab initio* simulation package (VASP) with the projector augmented wave (PAW) pseudo-potentials[41-43]. The generalized gradient approximation (GGA) with the Perdew-Burke-Ernzerhof (PBE) functional was adopted to treat the exchange correlation interactions[44]. The PBE functional has been previously found to essentially match the graphene cell parameter (2.46 Å)[11, 45], and also to successfully investigate the interaction between gas molecules and graphene doped metal atom[12, 21, 46-48]. The spin polarization was taken into account to gain the ground-state energy. Consistent with previous research models [49-52], a 4×4 supercell of graphene was built as catalyst supports and the vacuum layer was set to 15 Å to avoid the interaction among mirror images [49, 53].

Through the convergence test, the kinetic energy cutoff for the plane-wave basis set was chosen as 500 eV (as shown in Fig. S1 of supporting information). Gaussian smearing with a width of σ=0.05 eV was adopted for the occupation of the electronic levels[25, 54, 55]. For structure optimization, the positions of all atoms were allowed to fully relax with the conjugate gradient method until the maximum force on any atom was less than 0.02 eV/Å. Considering the computational time and accuracy, the Brillouin zone was sampled with a 7×7×1 Γ-centered k-point grid for structure optimization calculation, and k-point grid selection was tested until energy change was less than 10 meV/atom (as shown in Fig. S1 of supporting information). While a 15×15×1 Γ-centered k-point grid was used to calculate energy and density of states (DOS). Additionally, the convergence precision of total energy between two self-consistent steps was taken to be 10^{-5} eV for structure optimization and DOS calculation. In order to locate transition states, climbing-image nudged elastic band (CI-NEB) method was adopted with four images between the starting and ending geometries [34, 56, 57]. Frequency calculation was performed to confirm the accuracy of minima and transition states and to acquire zero point energy correction. There was no imaginary frequency in equilibrium structures, and there was only one imaginary frequency in transition state along the reaction path. In detail, the vibrational frequencies were obtained from numerical Hessian calculations with finite displacements of ±0.02 Å. Considering the computational accuracy and time, Hessians were calculated entirely for O_2 molecule but only partly for Fe/GS (Fe atom and the atoms adjacent to Fe atom). The previous study has indicated that such partial Hessian computations yield accurate vibrational frequencies[58].

The binding energy (E_b) between Fe adatom and substrates was defined as $E_b = E_{sub} + E_{Fe} - E_{sub+Fe}$, where E_{sub+Fe}, E_{sub} and E_{Fe} are the total energy of Fe/GS, graphene substrates and Fe atom, respectively. In addition, the adsorption energy (E_{ads}) of O_2 on Fe/GS was calculated to describe the interaction strength between gases and Fe/GS. It was calculated according to $E_{ads} = E_{Fe/GS} + E_{gas} - E_{gas-Fe/GS}$, where $E_{Fe/GS}$, E_{gas} and $E_{gas-Fe/GS}$ are the energy of Fe/GS, O_2 and adsorption systems, respectively. According to the calculation formula of binding energy and adsorption energy, a positive value of E_b or E_{ads} represents a stable adsorption, and a higher positive value of E_b or E_{ads} corresponds to a stronger interaction. The energy barrier (E_a) was calculated to examine the catalytic activity of Fe/GS and it can be obtained according to $E_a = E_{TS} - E_{IS}$, where E_{IS} and E_{TS} are the energy of reaction and transition state. The energies of isolated Fe atom and O_2 molecule were calculated in a large cell of 9.84 Å×9.84 Å×15 Å with only Γ point. In

View Article Online
DOI: 10.1039/C7CP08301G

addition, the binding energy, adsorption energy and energy barrier were calculated through zero point energy correction. Furthermore, Bader charge was calculated to analyze the electron transfer in quantity [59].

3. Results and discussion

3.1 Catalyst model

According to the number of doping nitrogen atom and vacancy, the geometric structures of single atom iron catalysts with ten kinds of graphene-based substrates were selected as research model, as shown in Fig. 1. In detail, for doping two nitrogen atoms, there are two kinds of configurations which are contraposition and ortho position. For ortho position, we select the highest stability configuration from two different configurations according to the research of Zhang[60]. The corresponding adsorption height of Fe atom, charge of Fe atom and binding energy are summarized in Table 1. In detail, according to the number of vacancy in graphene, we can divide Fe/GS into two groups, one is single atom iron catalysts with single vacancy graphene-based substrates (Fe/SV-GS), and the other is single atom iron catalysts with double vacancy graphene-based substrates (Fe/DV-GS). In Fig. 1, the number of nitrogen atom in Fe/SV-GS increases gradually from (a) to (d), and the number of nitrogen atom in Fe/DV-GS increases gradually from (e) to (j).

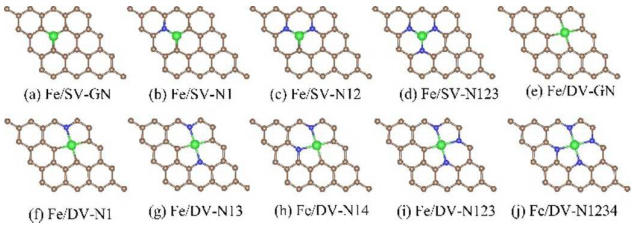

Fig. 1 The structures of single atom iron catalysts with different graphene-based substrates

Table 1 The adsorption height of Fe atom (h, Å), charge of Fe atom (q,e) and binding energy (E_b, eV) for Fe/GS. (The distance between Fe atom and substrates plane was defined as the adsorption height of Fe atom)

Fe/GS	h (Å)	q (e)	E_b (eV)
Fe/SV-GN	1.345(1.36[12])	+0.687	7.138(7.28[61])
Fe/SV-N1	1.312	+0.747	5.779
Fe/SV-N12	1.404	+0.840	5.219
Fe/SV-N123	1.230	+0.889	4.406
Fe/DV-GN	0.660(0.67[12])	+0.895	6.123(6.47[61])
Fe/DV-N1	0.555	+1.008	7.190
Fe/DV-N13	0.023	+1.100	7.564
Fe/DV-N14	0.066	+1.054	7.058
Fe/DV-N123	0.068	+1.061	7.391
Fe/DV-N1234	0.053(0.03[62])	+1.081	7.139(7.07[63])

The catalyst of Fe/SV-GN, Fe/DV-GN and Fe/DV-N1234 have been studied widely. The calculated structure parameter of Fe/SV-GN, Fe/DV-GN and Fe/DV-N1234 in this work corresponds well with the previous results, which can guarantee the rationality and validity of this calculated results. However, there is a difference of 0.35 eV between the calculated results and previous calculations[61], which seems to be caused by different surface coverage of Fe atom and calculation parameters. In the research of Liu [34], the charge of Pt atom is a good descriptor of adsorption and catalytic activation of O_2 in the system of Pt/GS, so the charge of Fe atom should be took into account. In Fe/SV-GS, with the number of doped nitrogen atoms increase, the charge of Fe atom increases gradually, indicating that the Fe/SV-GS will be more active with nitrogen atoms doping. In DV-GS, the charge of Fe atom shows an increasing tendency as the number of nitrogen atoms increases. Comparing Fe/SV-GS and Fe/DV-GS, the charge of Fe atom in Fe/DV-GS is bigger than that in Fe/SV-GS, which may suggest that Fe/DV-GS will be more active than Fe/SV-GS according to the research of Liu [34]. In addition, the adsorption height of Fe atom in Fe/DV-GS is obviously smaller than that in Fe/SV-GS, and the Fe atom almost locates in graphene plane when the number of nitrogen atoms reaches two in Fe/DV-GS.

As mentioned above, the stability is a key factor for SACs. Compared with the binding energy of Fe atom on perfect graphene (1.04 eV)[11], the binding energies of Fe/GS are all sufficiently large to anchor the catalyst atom. In order to further confirm the stability, the cohesive energy of Fe bulk in experiment was selected as a reference. The value of cohesive energy is 4.28 eV[64] which is smaller than the binding energies of Fe/GS, suggesting that Fe/GS should have high stability. In detail, a large change in binding energies of Fe/GS can be found. The binding energy of Fe/SV-GS decreases gradually with nitrogen atoms doping, while the binding energy of Fe/DV-GS increases slightly when nitrogen atom is doped in graphene-based substrates. In the research of Liu[34], the binding energies of Pt/SV-GS are -7.25 eV, -4.94 eV, -4.58 eV and -3.02 eV, respectively. The tendency of binding energy in Pt/SV-GS is the same as Fe/SV-GS and the variation of binding energy in Pt/SV-GS is 4.2 eV which is bigger than that of Fe/SV-GS, suggesting that the large change in binding energies under different graphene-based substrates is reasonable. Furthermore, the large variation of binding energy also suggests that the support effect of graphene-based substrates has a significant influence on the stability of SACs.

3.2 Adsorption of O_2 molecule on Fe/GS

In order to search the energetically most favorable adsorption configuration, horizontal and vertical initial configurations of O_2 molecule with different orientation were optimized, and the corresponding stable adsorption configuration are named as end-on and side-on adsorption model. The stable adsorption geometries of O_2 molecule on Fe/SV-GS and Fe/DV-GS are shown in Fig. 2 and Fig. 3, respectively. In addition, the adsorption geometric parameters and adsorption energies are summarized in Table S1.

View Article Online
DOI: 10.1039/C7CP08301G

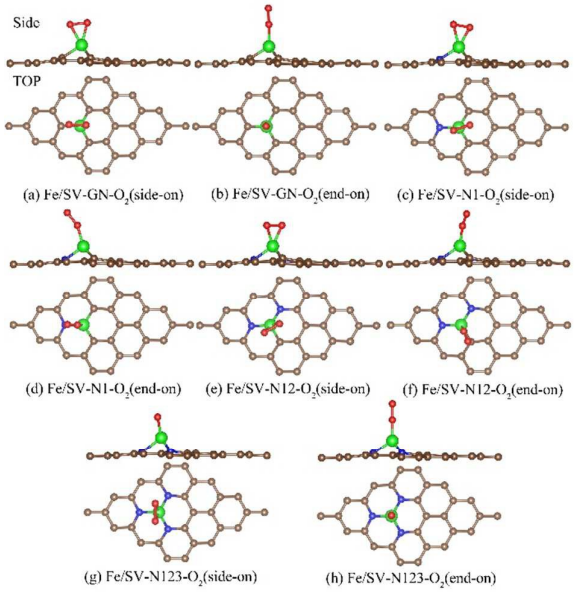

Fig. 2 The adsorption geometries of O_2 molecule on the surface of Fe/GN catalyst with single vacancy graphene

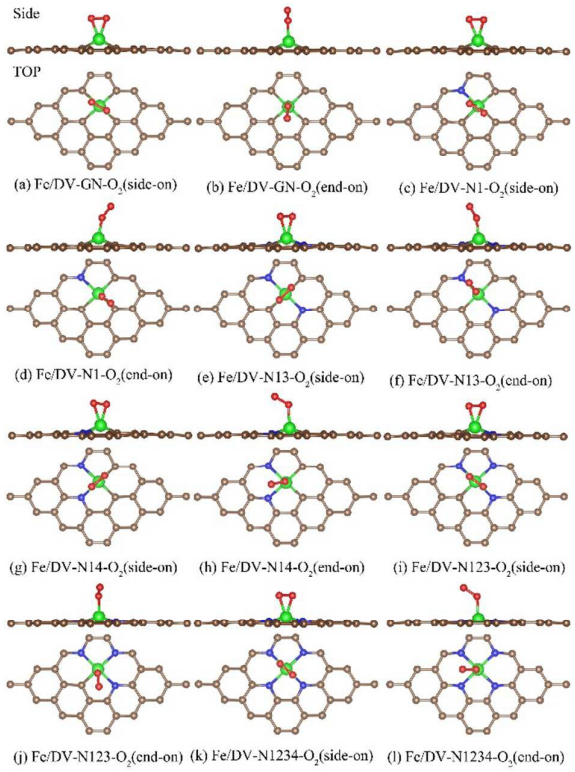

Fig. 3 The adsorption geometries of O_2 molecule on the surface of Fe/GN catalyst with double vacancy graphene

In order to further analyze the support effects on adsorption and catalytic activation of O_2, the most stable adsorption configurations of O_2 were selected as research objects, and the histogram of adsorption energies of O_2 on Fe/GS were plotted to analyze the support effects of graphene-based substrates on adsorption characteristics, as shown in Fig. 4.

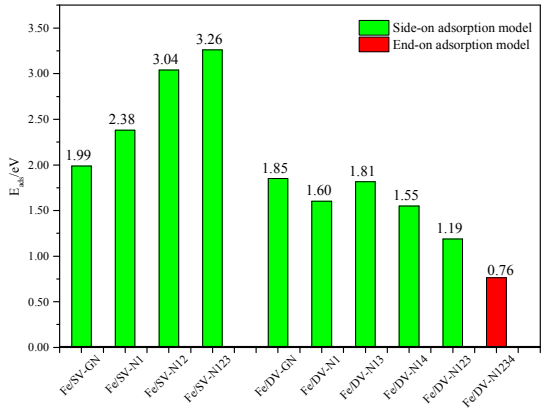

Fig. 4 The adsorption energies of O_2 under different Fe/GS

From Fig. 4, there is an obvious difference of adsorption energy of O_2 between different Fe/GS catalysts. It is worth noting that there is an interesting change of the most stable adsorption configuration of O_2 on Fe/GS. Apart from Fe/DV-N1234, the most stable adsorption configuration of O_2 on Fe/GS is side-on adsorption model. In detail, the adsorption energy of O_2 on Fe/SV-GS increases as the doping of nitrogen atom, while the adsorption energy of O_2 on Fe/DV-GS shows a gradual decreasing tendency. The adsorption energy of O_2 on Fe/SV-N123 is biggest, which indicates that Fe/SV-N123 may has high catalytic activation for O_2 dissociation. The adsorption characteristics of O_2 on Fe/GS suggested that support effect of graphene-based substrates has a significant influence on O_2 adsorption.

Combining the charge of Fe atom (Table 1) and corresponding adsorption energy of O_2, the adsorption energy of O_2 on Fe/SV-GS increases with the charge of Fe atom increases. In the research of Liu[34], there is an obviously positive correlation between the charge of Pt atom and corresponding adsorption energy of O_2 on the surface of Pt/GN catalysts, which suggests that the adsorption of O_2 on Fe/SV-GS is also mainly affected by the charge of Fe atom. However, there is no obvious relationship between the adsorption energy of O_2 on Fe/DV-GS and the charge of Fe atom, indicating that the adsorption of O_2 molecule on Fe/GS may be affected by other factor. Therefore, a further explanation for the difference of adsorption energy of O_2 between different Fe/GS should be conducted.

Considering that the bond length of two oxygen atoms can be an indicator of O_2 activation and there may be a positive correlation between adsorption energy of O_2 and bond length of two oxygen atoms [46], the relationship of adsorption energy and bond length was investigated, as shown in Fig. 5. From Fig. 5, strong positive correlation of adsorption energy and bond length can be found, with the square of correlation coefficient is 0.75, so the bond length of O_2 seems to be a descriptor of adsorption strength.

View Article Online
DOI: 10.1039/C7CP08301G
Journal Name ARTICLE

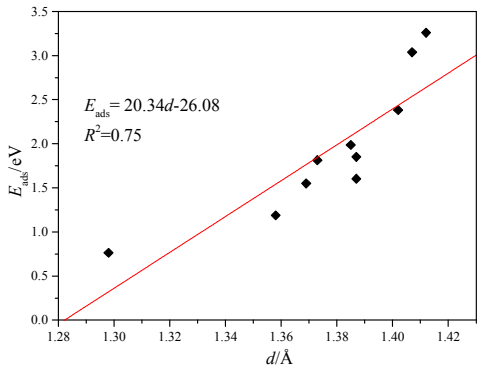

Fig. 5 The adsorption energies of O_2 as a function of bond length of O_2

The electron transfer is a key factor for understanding chemical adsorption and reaction process. For instance, there are two different electron transfer mechanisms under an external electric field in adsorption of O_2 on Au/GS[46]. Therefore, in order to analyze the mechanisms of electron transfer in the adsorption process, the charge change before and after adsorption of O_2 (Δq-O_2, e), Fe atom (Δq-Fe, e) and graphene substrate (Δq-sub, e) were plotted in Fig. 6, and the detail data were provided in Table S2.

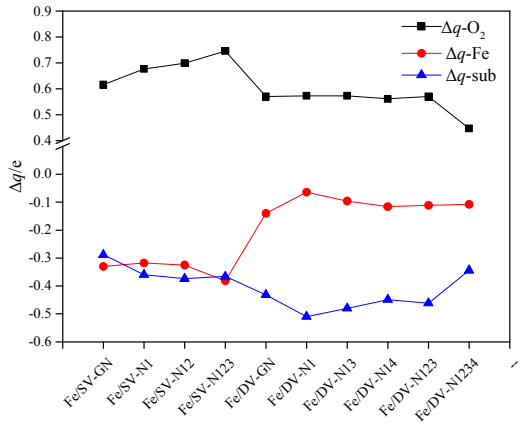

Fig. 6 The scatter diagram of the valence electron variation of O_2, Fe and graphene substrates

From Fig. 6, O_2 molecule always gains electron, while Fe atom and graphene substrates always loss electron in the adsorption of O_2 on Fe/GS. The number of electron gain of O_2 in Fe/SV-GS increases gradually as the doping of nitrogen atom, while there is no obvious variation tendency in Fe/DV-GS. O_2 acts as the electron adopter and Fe atom and graphene-based substrates act as the electron donor in the adsorption of O_2 on Fe/SV-GS, and the number of donor electron of Fe atom and graphene substrates are about the same. However, in Fe/DV-GS, the number of donor electron of graphene substrates is much larger than that of Fe atom, indicating that graphene substrates act as the electron donor and the Fe atom is mainly acts as the bridge of electron transfer. In particular, the number of donor electron of Fe atom is 0.064 e (From Table S2) which is accounts for only 1% of the gain electron of O_2 in the adsorption of O_2 on Fe/DV-N1. In summary, graphene-based substrates and Fe atom act as electron donor in the adsorption of O_2 on Fe/SV-GS, while Fe atom mainly act as bridge of electron transfer in the adsorption of O_2 on Fe/DV-GS. Furthermore, the graphene-based substrates not only act as anchoring effect of catalyst atom, but also participate in the adsorption of O_2 through donating electrons to O_2 molecule.

Overall, there are two key issues need to be further discussed: one is the reason why the end-on adsorption configuration is preferred only on Fe/DV-N1234, the other one is the relationship between support effect of graphene-based substrates and adsorption energy of O_2. In order to analyze the issue, frontier molecular orbital and electronic structure analysis have been performed.

3.3 Frontier molecular orbital analysis

From the above analysis, there is an obvious electron transfer between O_2 molecule and Fe/GS, and the direction of electron transfer is from Fe atom and graphene-based substrates to O_2 molecule. In detail, we can conclude that the electron at the valence band maximum (VBM) of Fe/GS transfers to the lowest unoccupied molecular orbital (LUMO) of O_2 molecule in the process of electron transfer. Considering that the bonding process should follow the symmetrical matching principle in frontier molecular orbital method[65], we examined the frontier molecular orbital distribution of O_2 molecule and Fe/GS. The density of states and frontier molecular orbital distribution of O_2 molecule was plotted in Fig. 7. From Fig. 7, the positive and negative phases of wavefunction are plotted in red and blue respectively and there is an obvious difference between the HOMO and LUMO of O_2 molecule in wavefunction distribution. According to the symmetrical matching principle, if the most stable adsorption configuration of O_2 on Fe/DV-N1234 is end-on adsorption model, the wavefunction distribution of Fe/DV-N1234 at VBM should only has one phase of wavefunction.

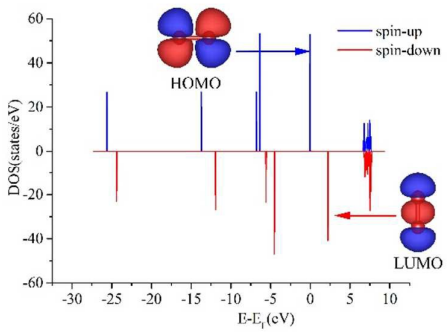

Fig. 7 The density of states and frontier molecular orbital distribution of O_2. (The contour lines in plots are drawn at 0.03 e/Å^3 intervals)

In order to validate this suppose, the wavefunction distribution of Fe/GS at VBM has been plotted in Fig. 8 and Fig. S2. From Fig. 8, the wavefunction of Fe/DV-N1234 at VBM has only one phase, while the wavefunction of other Fe/GS at VBM

View Article Online
DOI: 10.1039/C7CP08301G

has two phase. Therefore, the most stable adsorption configuration of O_2 on Fe/DV-N1234 is end-on adsorption model can be well understood through symmetrical matching principle in frontier molecular orbital method.

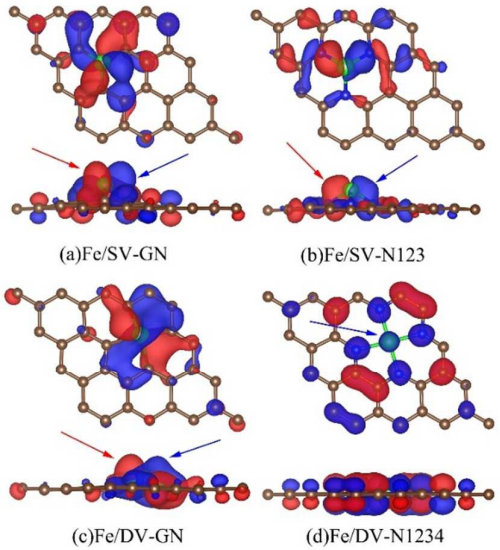

Fig. 8 The wavefunction distribution of valence band maximum (VBM) of four typical Fe/GS. (The contour lines in plots are drawn at 0.03 *e*/Å^3 intervals)

3.4 Electronic structure analysis

Since the Fe/GS are composed of the same catalyst atom (Fe) and different graphene-based supports, the difference of adsorption energy between Fe/GS should originate from the effect of graphene-based substrates. Furthermore, it is known that there is a close relationship between the support effect and electronic structure of catalysts. Therefore, the electronic structure analysis of Fe/GS was performed to understand the nature relationship between the support effect of graphene-based substrates and adsorption energy, and Fermi softness and work function were calculated for electronic structure analysis.

According to frontier molecular orbital theory, the whole frontier electronic band of the solid surface is reactive. It is known that the closer the electronic state to the Fermi level, the greater the contribution to bonding interaction. Therefore, the reactivity of a catalyst should be determined by both density of states ($g(E)$) and a weight function ($W(E)$) which quantifies the contribution of every electronic state to the surface bonding [66]. According to this idea, Fermi softness (S_F), which can describe the chemical reactivity of solid surfaces in quantity, is proposed by the research group of Zhuang[66], and the S_F can be calculated from the following equation:

$$S_F = \int_{-\infty}^{+\infty} g(E) W(E) dE \quad (1)$$

Where $g(E)$ is the total density of states. $W(E)$ can be acquired from the derivative of the Fermi-Dirac function, $-f_T'(E-E_F)$. The $-f_T'(E-E_F)$ is defined as the following equation:

$$-f_T'(E-E_F) = \frac{1}{kT} \cdot \frac{1}{\left(e^{(E-E_F)/kT}+1\right)\left(e^{(E_F-E)/kT}+1\right)} \quad (2)$$

Where kT is the nominal electron temperature (k is the Boltzmann constant and T is parametric temperature)[66]. According to the calculation formula of Fermi softness, T is just a parameter to control the distribution of weight function, suggesting that T cannot compare with the true temperature. In addition, $W(E)$ is affected by the value of kT, so the value of kT has a significant influence on Fermi softness.

From the calculation According the research of Zhuang[66], the selection of kT depends on adsorbates, indicating that the value of kT between different adsorption systems should have a difference. The value of kT in the adsorption of H atom on VS_2[67] is 0.4 eV, while the value of kT in the adsorption of toxic gases (NO_2, NH_3, SO_3 and H_2S) on single atom iron catalyst[25] is 0.25 eV. Therefore, it is necessary to choose an appropriate value of kT before applying Fermi softness to analyze the activity of catalyst.

To gain the optimal value of kT and investigate the effect of kT on Fermi softness, we calculate the Fermi softness under different values of kT according to the method of Zhuang[66]. The optimal value of kT can be determined according to the corresponding square of correlation coefficient (R^2) between adsorption energy and Fermi softness. The value of S_F and R^2 for ten kinds of Fe/GS under different kT were plotted in Fig. 9.

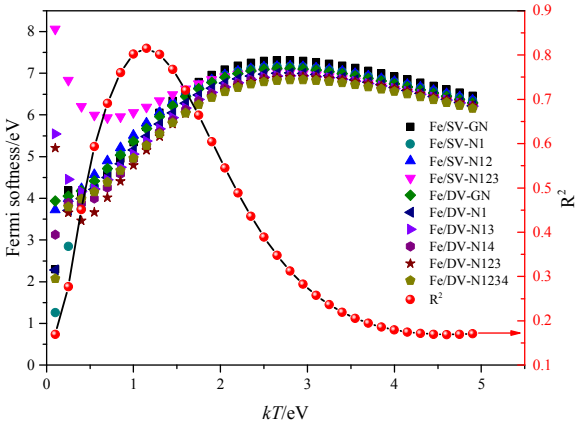

Fig. 9 Fermi softness and the square of correlation coefficient under different kT

From Fig. 9, the R^2 between adsorption energy and Fermi softness vary significantly with the value of kT, suggesting that the choice of kT is crucial for Fermi softness analysis. In detail, R^2 increases first and then decreases with the increase of kT, and R^2 reaches the maximum value when kT is 1.15 eV. Therefore, we selected 1.15 eV as the optimal value of kT, and Fermi softness of Fe/GS with optimal value of kT was summarized in Table S3. Furthermore, the liner fitting between adsorption energy and Fermi softness was performed, as shown in Fig. 10. Form Fig. 10, the value of R^2 under optimum condition is 0.81, indicating that Fermi softness can be an efficient descriptor of adsorption energy.

View Article Online
DOI: 10.1039/C7CP08301G

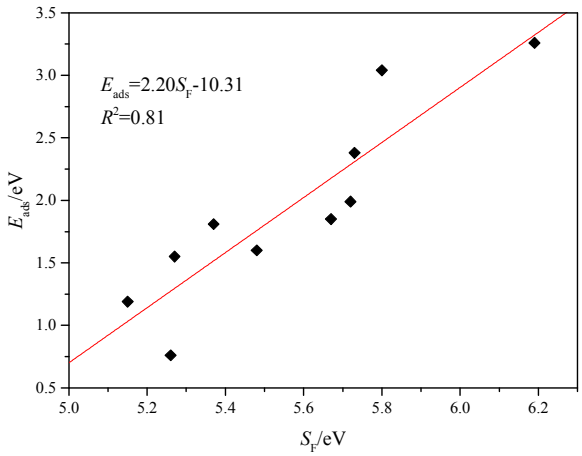

Fig. 10 The adsorption energy of O_2 as a function of Fermi softness

Shen et al. investigated the adsorption of O, OH and OOH on seven different metal surfaces and proposed that ionic bonding energy (E_{ionic}) can be used as an effective descriptor for adsorption energy in ionic bonding system[68]. The calculation of E_{ionic} can be defined as:

$$E_{ionic} = \Delta q \times \Delta \Phi = \Delta q \times (\Phi - \Phi_0) \quad (3)$$

Where Δq is the amount of electron transfer, Φ and Φ_0 are the work function of Fe/GS and O_2 molecule, respectively. In detail, the work function (Φ) and be obtained from the following equation:

$$\Phi = E_V - E_F \quad (4)$$

Where E_V and E_F are the vacuum level and Fermi level, respectively. In order to further verify and broaden the applicability of this method, the method was applied to explain the relationship between adsorption energy and support effect. The detail data of E_{ionic} for different Fe/GS was summarized in Table S3, and the liner fitting between adsorption energy and E_{ionic} was performed, as shown in Fig. 11.

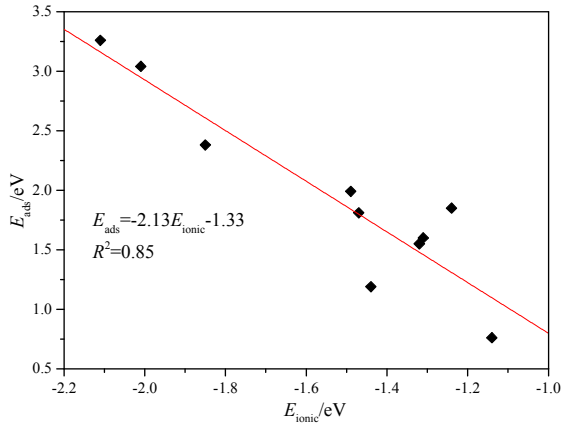

Fig. 11 The adsorption energy of O_2 as a function of work function

From Fig. 11, an obvious correlation between adsorption energy and work function can be found, with R^2 value of 0.85, indicating that the work function is also a good descriptor of adsorption energy in the system of Fe/GS. Compared with Fermi softness analysis, work function is not dependent on given parameter (kT), so it is more direct and effective for analyzing the adsorption of O_2 on the surface of Fe/GS.

3.4 Catalytic activation of O_2 analysis

In order to further examine the activity of Fe/GS in catalytic activation of O_2, the most stable adsorption configuration of O_2 on Fe/GS were selected to investigate the dissociation reaction of O_2 molecule. The dissociation reaction of O_2 molecule on Fe/GS has been systematically studied through CI-NEB method, and the detail reaction path and transition state structures have been plotted in Fig. S3 and Fig. S4. To analyze energy barrier, the potential energy surfaces were plotted, as shown in Fig. 12. From Fig. 12, the energy barrier of O_2 dissociation on Fe/SV-N123 is the smallest, and the value is 1.12 eV which is close to the energy barrier of O_2 dissociation on Pt/SV-N123 (1.09 eV)[34], indicating that the catalytic activity of Fe/GS can be compared with precious metals. Different from the dissociation reaction of O_2 on Pt/GS[34], the dissociation reaction of O_2 on Fe/GS (apart from Fe/SV-N1 and Fe/DV-N123) is exothermic, which indicates that the dissociation reaction of O_2 on Fe/GS (expect Fe/SV-N1 and Fe/DV-N123) may take place spontaneously. Combining the performance in adsorption and activation of O_2, we can conclude that Fe/GS, especially Fe/SV-N123, is a kind of promising catalyst for adsorption and catalytic activation of O_2 molecule which is hopeful to replace the noble metal.

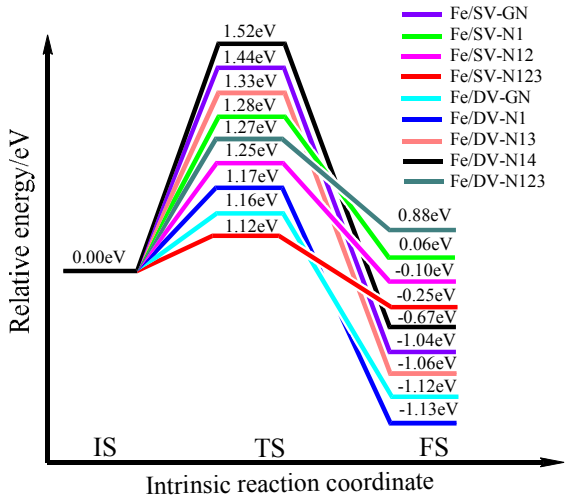

Fig. 12 Potential energy surfaces for dissociation reaction of O_2 on Fe/GS

Conclusions

Adsorption configuration, electron transfer mechanism, adsorption energy and energy barrier have been studied in the

View Article Online
DOI: 10.1039/C7CP08301G

present work to investigate the support effect of graphene-based substrates on adsorption and catalytic activation of O_2. Stemming from the above calculation and discussion, we can conclude that the support effects of graphene-based substrates have an obvious influence on the stability of SACs, adsorption and catalytic activation of O_2, mainly in adsorption configuration, electron transfer mechanism, adsorption energy and energy barrier. The difference of stable adsorption configuration of O_2 on Fe/GS can be well understood through symmetrical matching principle in frontier molecular orbital method. Two different mechanisms of electron transfer between O_2 and Fe/GS are also revealed, Fe atom acts as electron donor in Fe/SV-GS while Fe atom mainly acts as bridge of electron transfer in Fe/DV-GS. Furthermore, Fermi softness and work function are good descriptors of adsorption energy and can well reveal the relationship between electronic structure and adsorption. Moreover, Fe/SV-N123 is a promising non-noble-metal single atom catalyst in adsorption and catalytic oxidation of O_2 according to the adsorption energy and energy barrier of O_2. We hope this work can provide a deep insight into the support effects on O_2 activation and a guideline for development and design of new non-noble-metal single atom catalysts.

Conflicts of interest

There are no conflicts to declare.

Acknowledgements

This work was supported by the National Natural Science Foundation of China (No. 91545122) and the Fundamental Research Funds for the Central Universities (JB2015RCY03 and 2017XS121). The wavefunction plots were drawn with the help of the vaspmo program developed by Yang Wang. Computational resources from the Lvliang Supercomputer Center were acknowledged.

Notes and references

1. B. Qiao, A. Wang, X. Yang, L. F. Allard, Z. Jiang, Y. Cui, J. Liu, J. Li and T. Zhang, *Nat. Chem.*, 2011, **3**, 634-641.
2. B. Qiao, J.-X. Liang, A. Wang, J. Liu and T. Zhang, *Chin. J. Catal.*, 2016, **37**, 1580-1586.
3. Y. Lou and J. Liu, *Ind. Eng. Chem. Res.*, 2017, **56**, 6916-6925.
4. M. Yang, J. Liu, S. Lee, B. Zugic, J. Huang, L. F. Allard and M. Flytzani-Stephanopoulos, *J. Am. Chem. Soc.*, 2015, **137**, 3470-3473.
5. M. Flytzani-Stephanopoulos, *Acc. Chem. Res.*, 2014, **47**, 783-792.
6. S. Back, J. Lim, N. Y. Kim, Y. H. Kim and Y. Jung, *Chem. Sci.*, 2017, **8**, 1090-1096.
7. X. Li, W. Bi, L. Zhang, S. Tao, W. Chu, Q. Zhang, Y. Luo, C. Wu and Y. Xie, *Adv. Mater.*, 2016, **28**, 2427-2431.
8. X. Chen, L. Yu, S. Wang, D. Deng and X. Bao, *Nano Energy*, 2017, **32**, 353-358.
9. F. Li, H. Shu, C. Hu, Z. Shi, X. Liu, P. Liang and X. Chen, *ACS Appl. Mater. Interfaces*, 2015, **7**, 27405-27413.
10. F. Dvorak, M. Farnesi Camellone, A. Tovt, N. D. Tran, F. R. Negreiros, M. Vorokhta, T. Skala, I. Matolinova, J. Myslivecek, V. Matolin and S. Fabris, *Nat. Commun.*, 2016, **7**, 10801.
11. M. Manadé, F. Viñes and F. Illas, *Carbon*, 2015, **95**, 525-534.
12. A. V. Krasheninnikov, P. O. Lehtinen, A. S. Foster, P. Pyykko and R. M. Nieminen, *Phys. Rev. Lett.*, 2009, **102**, 126807.
13. S. Kim, P. Gamallo, F. Viñes, J. Y. Lee and F. Illas, *Theor. Chem. Acc.*, 2017, **136**.
14. B. Bayatsarmadi, Y. Zheng, A. Vasileff and S.-Z. Qiao, *Small*, 2017, **13**, 1700191.
15. B. F. Machado and P. Serp, *Catal. Sci. Technol.*, 2012, **2**, 54-75.
16. X. Zhang, Z. Lu and Z. Yang, *J. Mol. Catal. A: Chem.*, 2016, **417**, 28-35.
17. W. Kiciński, B. Dembinska, M. Norek, B. Budner, M. Polański, P. J. Kulesza and S. Dyjak, *Carbon*, 2017, **116**, 655-669.
18. C. Li, *Chin. J. Catal.*, 2016, **37**, 1443-1445.
19. D. Deng, X. Chen, L. Yu, X. Wu, Q. Liu, Y. Liu, H. Yang, H. Tian, Y. Hu and P. Du, *Sci. Adv.*, 2015, **1**, e1500462.
20. X. Zhang, J. Guo, P. Guan, C. Liu, H. Huang, F. Xue, X. Dong, S. J. Pennycook and M. F. Chisholm, *Nat. Comm.*, 2013, **4**, 1924.
21. L. Wang, Q. Luo, W. Zhang and J. Yang, *Int. J. Hydrogen Energy*, 2014, **39**, 20190-20196.
22. E. Ashori, F. Nazari and F. Illas, *Phys. Chem. Chem. Phys.*, 2017, **19**, 3201-3213.
23. Y. Tang, Z. Liu, Z. Shen, W. Chen, D. Ma and X. Dai, *Sens. Actuators, B*, 2017, **238**, 182-195.
24. D. Cortés-Arriagada, N. Villegas-Escobar and D. E. Ortega, *Appl. Surf. Sci.*, 2018, **427**, 227-236.
25. Z. Gao, W. Yang, X. Ding, G. Lv and W. Yan, *Appl. Surf. Sci.*, 2018, **436**, 585-595.
26. X. Zhang, S. Yu, H. Chen and W. Zheng, *RSC Adv.*, 2015, **5**, 82804-82812.
27. Y. Tang, S. Zhao, B. Long, J.-C. Liu and J. Li, *J. Phys. Chem. C*, 2016, **120**, 17514-17526.
28. X. F. Yang, A. Q. Wang, B. T. Qiao, J. Li, J. Y. Liu and T. Zhang, *Acc. Chem. Res.*, 2013, **46**, 1740-1748.
29. S. Liang, C. Hao and Y. Shi, *ChemCatChem*, 2015, **7**, 2559-2567.
30. X. Ding, Z. Li, J. Yang, J. G. Hou and Q. Zhu, *J. Chem. Phys.*, 2004, **120**, 9594-9600.
31. C. Zhang, B. Yoon and U. Landman, *J. Am. Chem. Soc.*, 2007, **129**, 2228-2229.
32. B. Yoon, H. Hakkinen, U. Landman, A. S. Worz, J. M. Antonietti, S. Abbet, K. Judai and U. Heiz, *Science*, 2005, **307**, 403-407.
33. F. He, K. Li, C. Yin, Y. Wang, H. Tang and Z. Wu, *Carbon*, 2017, **114**, 619-627.
34. S. G. Liu and S. P. Huang, *Carbon*, 2017, **115**, 11-17.
35. L. Wang, H. Li, W. Zhang, X. Zhao, J. Qiu, A. Li, X. Zheng, Z. Hu, R. Si and J. Zeng, *Angew. Chem.*, 2017, **56**, 4712-4718.
36. X. Zhang, Z. Lu, G. Xu, T. Wang, D. Ma, Z. Yang and L. Yang, *Phys. Chem. Chem. Phys.*, 2015, **17**, 20006-20013.
37. X. Liu, Y. Sui, T. Duan, C. Meng and Y. Han, *Catal. Sci. Technol.*, 2015, **5**, 1658-1667.

View Article Online
DOI: 10.1039/C7CP08301G

38. X. Liu, Y. Sui, T. Duan, C. Meng and Y. Han, *Phys. Chem. Chem. Phys.*, 2014, **16**, 23584-23593.
39. X. Liu, K. X. Yao, C. Meng and Y. Han, *Dalton Trans.*, 2012, **41**, 1289-1296.
40. X. Liu, C. Meng and Y. Han, *Nanoscale*, 2012, **4**, 2288-2295.
41. G. Kresse and D. Joubert, *Phys. Rev. B*, 1999, **59**, 1758.
42. G. Kresse and J. Furthmüller, *Comput. Mater. Sci.*, 1996, **6**, 15-50.
43. G. Kresse and J. Furthmüller, *Phys. Rev. B*, 1996, **54**, 11169.
44. J. P. Perdew, K. Burke and M. Ernzerhof, *Phys. Rev. Lett.*, 1996, **77**, 3865.
45. P. Janthon, F. Vines, S. M. Kozlov, J. Limtrakul and F. Illas, *J. Chem. Phys.*, 2013, **138**, 244701.
46. T. Zhang, Q. Xue, M. Shan, Z. Jiao, X. Zhou, C. Ling and Z. Yan, *J. Phys. Chem. C*, 2012, **116**, 19918-19924.
47. X. Liu, C. Meng and Y. Han, *Phys. Chem. Chem. Phys.*, 2012, **14**, 15036-15045.
48. Y. Li, Z. Zhou, G. Yu, W. Chen and Z. Chen, *J. Phys. Chem. C*, 2010, **114**, 6250-6254.
49. Y. Tang, W. Chen, C. Li, L. Pan, X. Dai and D. Ma, *Appl. Surf. Sci.*, 2015, **342**, 191-199.
50. Y. Lee, S. Lee, Y. Hwang and Y.-C. Chung, *Appl. Surf. Sci.*, 2014, **289**, 445-449.
51. M. Sun, W. Tang, Q. Ren, S. Wang, JinYu, Y. Du and Y. Zhang, *Appl. Surf. Sci.*, 2015, **356**, 668-673.
52. Z. Gao, W. Yang, X. Ding, G. Lv and W. Yan, *Appl. Surf. Sci.*, DOI: https://doi.org/10.1016/j.apsusc.2017.12.077.
53. L. Ma, J.-M. Zhang, K.-W. Xu and V. Ji, *Appl. Surf. Sci.*, 2015, **343**, 121-127.
54. X. Wang, H. Zhou, Z. Yan, X. Zhang, J. Jia and H. Wu, *Theor. Chem. Acc.*, 2017, **136**.
55. K. T. Chan, J. B. Neaton and M. L. Cohen, *Phys. Rev. B*, 2008, **77**.
56. G. Henkelman, B. P. Uberuaga and H. Jónsson, *J Chem. Phys.,* 2000, **113**, 9901-9904.
57. G. Henkelman and H. Jónsson, *J Chem. Phys.*, 2000, **113**, 9978-9985.
58. C. Riplinger and E. A. Carter, *J Phys. Chem. C*, 2015, **119**, 9311-9323.
59. W. Tang, E. Sanville and G. Henkelman, *J. Phys.: Condens. Matter*, 2009, **21**, 084204.
60. J. Zhang, Y. Wang, Z. Zhu and M. Zhang, *J. Mol. Model.*, 2017, **23**, 170.
61. Y. Tang, J. Zhou, Z. Shen, W. Chen, C. Li and X. Dai, *RSC Adv.*, 2016, **6**, 93985-93996.
62. A. T. Lee, J. Kang, S.-H. Wei, K. J. Chang and Y.-H. Kim, *Phys. Rev. B*, 2012, **86**.
63. S. Kattel, P. Atanassov and B. Kiefer, *J Phys. Chem. C*, 2012, **116**, 8161-8166.
64. P. Janthon, S. M. Kozlov, F. Vines, J. Limtrakul and F. Illas, *J. Chem. Theory Comput.*, 2013, **9**, 1631-1640.
65. K. Fukui, *science*, 1982, **218**, 747-754.
66. B. Huang, L. Xiao, J. Lu and L. Zhuang, *Angew. Chem.*, 2016, **55**, 6239-6243.
67. Y. Zhang, X. S. Chen, Y. Huang, C. Zhang, F. Li and H. B. Shu, *J. Phys. Chem. C*, 2017, **121**, 1530-1536.
68. X. C. Shen, Y. B. Pan, B. Liu, J. L. Yang, J. Zeng and Z. M. Peng, *Physi. Chem. Chem. Phys.,* 2017, **19**, 12628-12632.